Atlantic effects on recent decadal trends in global monsoon

Youichi Kamae[1,2*], Xichen Li[3,2], Shang-Ping Xie[2], and Hiroaki Ueda[1]

[1]Faculty of Life and Environmental Sciences, University of Tsukuba, Tsukuba, Ibaraki, Japan

[2]Scripps Institution of Oceanography, University of California San Diego, La Jolla, California, USA

[3]Institute of Atmospheric Physics, Chinese Academy of Sciences, Beijing, China

Submitted to *Climate Dynamics*

*Corresponding author: Youichi Kamae, Faculty of Life and Environmental Sciences, University of Tsukuba, 1-1-1 Tennoudai, Tsukuba, Ibaraki 305-8506, Japan (kamae.yoichi.fw@u.tsukuba.ac.jp), Tel.: +81-29-853-4757 Fax: +81-29-853-6709

Abstract

Natural climate variability contributes to recent decadal climate trends. Specifically the trends during the satellite era since 1979 include Atlantic and Indian Ocean warming and Pacific cooling associated with phase shifts of the Atlantic Multidecadal Oscillation and the Pacific Decadal Oscillation, and enhanced global monsoon (GM) circulation and rainfall especially in the Northern Hemisphere. Here we evaluate effects of the oceanic changes on the global and regional monsoon trends by partial ocean temperature restoring experiments in a coupled atmosphere–ocean general circulation model. Via trans-basin atmosphere–ocean teleconnections, the Atlantic warming drives a global pattern of sea surface temperature change that resembles observations, giving rise to the enhanced GM. The tropical Atlantic warming and the resultant Indian Ocean warming favor subtropical deep-tropospheric warming in both hemispheres, resulting in the enhanced monsoon circulations and precipitation over North America, South America and North Africa. The extratropical North Atlantic warming makes an additional contribution to the monsoon enhancement via Eurasian continent warming and resultant land–sea thermal gradient over Asia. The results of this study suggest that the Atlantic multidecadal variability can explain a substantial part of global climate variability including the recent decadal trends of GM.

Keywords: Global monsoon, PDO, AMO, meridional thermal gradient

1. Introduction

Monsoons develop over tropical-to-subtropical land and adjacent ocean regions (North and South America, North and South Africa, South and East Asia and Australia) and are characterized by salient seasonal variations in atmospheric circulation and precipitation (e.g. Murakami and Matsumoto 1994; Webster et al. 1998; Webster 2006). These seasonally reversing atmospheric overturning circulations throughout the tropics may be viewed as a "global monsoon" (GM) system (e.g. Trenberth et al. 2000; Wang and Ding 2008; Wang et al. 2014; An et al. 2015). The GM system varies on a wide range of timescales both naturally and in response to external forcing such as Earth's orbital parameters (associated with paleo-monsoon variability; Wang et al. 2014; Jiang et al. 2015; Yan et al. 2016) and anthropogenic radiative forcing agents (detailed below). Christensen et al. (2014) reviewed historical variations and future projections of GM by atmosphere–ocean coupled general circulation models (AOGCMs; e.g. Hsu et al. 2012, 2013; Kitoh et al. 2013; Lee and Wang 2014; Endo and Kitoh 2014). Since the early 20th century, substantial decadal-to-multidecadal variations in the GM subsystems have been reported, implying the importance of natural climate variability for historical GM variations.

The large-scale horizontal thermal gradient between land and ocean is a primal driver of the monsoon system. Meridional thermal gradient (MTG), measured by the gradient of middle to upper tropospheric temperature over South Asia and the tropical Indian Ocean (IO), is an useful index for Asian monsoon intensity (Li and Yanai 1996; Kawamura 1998; Arai and Kimoto 2008; Dai et al. 2013). Monsoon itself also affects the MTG via condensation heat release in the troposphere, resulting in a positive feedback between the monsoon and MTG (e.g. Li and Yanai 1996). Such deep-tropospheric land–sea thermal gradient tracks Asian monsoon

variability (Zuo et al. 2013; Roxy et al. 2015), projected future change (Ueda et al. 2006; Sun et al. 2010; Dai et al. 2013; Ma and Yu 2014; Ogata et al. 2014; Kamae et al. 2014b; Sooraj et al. 2015), and past climate changes (e.g. Ueda et al. 2011; Man et al. 2012).

The deep-tropospheric thermal gradient and monsoon systems are sensitive to spatial patterns of aerosols forcing and sea surface temperature (SST) anomaly (e.g. Kamae et al. 2015; Dong et al. 2016). Anthropogenic aerosols affect regional precipitation (e.g. Rotstayn and Lohmann 2002; Hwang et al. 2013; Wang et al. 2016) over the Asian (e.g. Bollasina et al. 2011; Dong et al. 2016) and African monsoon regions (e.g. Rotstayn et al. 2000; Rotstayn and Lohmann 2002; Kawase et al. 2011). Polson et al. (2014) pointed out that aerosols are fundamental drivers for the observed long-term weakening trend in GM rainfall since the mid-20th century. They also noted that the current AOGCMs still have limited representation of indirect effects of aerosols (Stevens and Feingold 2009), indicating that total aerosols effects on monsoons are still uncertain. Decadal trends in anthropogenic aerosols are weak since 1979 (Fig. 1b in Polson et al. 2014), a period with increased GM rainfall (Wang and Ding 2006; Hsu et al. 2011; Wang et al. 2012, 2013; Polson et al. 2014) particularly over the Northern Hemisphere (NH).

The recent decadal SST trend since 1979 (Fig. 1a) are influenced by basin-scale multidecadal variability modes: Interdecadal Pacific Oscillation (IPO) or Pacific Decadal Oscillation (PDO) and Atlantic Multidecadal Oscillation (AMO; e.g. Power et al. 1999; Deser et al. 2004; Newman et al. 2016). The tropical SST trends feature warming over the tropical Atlantic, IO, and western Pacific (IOWP) and cooling over the eastern Pacific (e.g. Luo et al. 2012; Watanabe et al. 2014; McGregor et al. 2014; Li et al. 2016). These SST trends are of great

70 importance for the decadal trends in global-mean surface air temperature (e.g. Kosaka and Xie 2013; Watanabe
71 et al. 2013; Li et al. 2016) and global atmospheric circulations including monsoons (Wang et al. 2012, 2013;
72 Trenberth et al. 2014; Ueda et al. 2015). Through partial ocean temperature restoring experiments, McGregor et
73 al. (2014), Li et al. (2016), and Kucharski et al. (2016) showed that tropical Atlantic SST can explain a
74 substantial part of the recent decadal variations of the tropical SST and atmospheric overturning circulation. The
75 partial temperature restoring technique is effective to examine local and remote influences of the oceans on the
76 monsoons and avoids the ambiguity in causality of SST variations over the warm oceans that is present in
77 atmosphere-only simulations with prescribed SST (Wang et al. 2005).

78 This study examines how recent SST change (for 1979–2012) in each tropical ocean basin (Atlantic, IO
79 and Pacific) affects the GM and its subsystems through the ocean temperature restoring experiments.
80 Atmospheric general circulation models are often used to quantify SST contributions from individual basins but
81 the results do not consider coupled inter-basin interactions; on interannual timescales, for example, SST
82 anomalies over the IO and Atlantic are forced by El Niño Southern Oscillation (ENSO) in the Pacific (e.g.
83 Chikamoto et al. 2015; Li et al. 2016). In addition, the IO and Atlantic SST also affect the ENSO amplitude and
84 frequency (Terray et al. 2015). Here we adopt the partial coupling method to explore the effect of cross-basin
85 interactions on the recent trends of the GM. We also apply the MTG-view for a physical interpretation on the
86 decadal GM trend. Section 2 describes the data and methods including model experiments and observations used
87 in this study. Section 3 presents the decadal climate trends over the tropics in SST and monsoon precipitation.

88 Section 4 compares regional patterns of trends between MTG, monsoon circulation and precipitation. Section 5
89 is a summary with discussions.

90

91 **2. Data and methods**

92 **2.1. Observations and reanalysis**

93 To examine decadal climate trends for 1979–2012, we used observed SST dataset (HadISST; Rayner et al.
94 2003) which was also used for model simulations (Sect. 2.2). We used three precipitation datasets (CRU TS
95 v3.23; Harris et al. 2014, Global Precipitation Climatology Project; hereafter GPCP; Huffman et al. 2009, and
96 the CPC Merged Analysis of Precipitation; hereafter CMAP; Xie and Arkin 1997) to evaluate observational
97 uncertainty (i.e. spread among datasets) in decadal trend of summertime precipitation. Three dimensional
98 atmospheric variables were derived from ERA-Interim (Dee et al. 2011) that well reproduces the interannual
99 variability and trend of the GM system since 1979 (Lin et al. 2014).

100 The monsoon domains are determined by an annual range of precipitation. In this study, areas where the
101 annual range of climatological GPCP precipitation (1979–2012) is greater than 2.5 mm day^{-1} are defined as
102 monsoon domains, similar to Kitoh et al. (2013). We mainly focus on land monsoon to examine remote influence
103 of restored ocean temperature on land rainfall (Sect. 2.2). The GM domain consists of seven subdomains: North
104 American Monsoon (NAM); South American Monsoon (SAM); North African Monsoon (NAF); South African
105 Monsoon (SAF); South Asian Monsoon (SAS); East Asian Monsoon (EAS); and Australian Monsoon (AUS; see

106 Sect. 3.2). For regional division, 20°N and 100°E are used to separate SAS from EAS (Fig. 5 in Kitoh et al.
107 2013).

108 In this study, decadal trends are calculated by low-pass-filtered (3-yr running mean) variables for 1979–
109 2012. The 3-yr running mean can largely remove interannual variability including the effect of ENSO (Wang et
110 al. 2013) and increase signal-to-noise ratio in decadal trends. We confirmed that large-scale patterns of decadal
111 trends were not sensitive to smoothing time windows (e.g. 5-yr running mean) of low-pass filter. We examine
112 summer monsoons by local summer mean determined by May to September in the NH and November to March
113 in the Southern Hemisphere (SH).

114

115 **2.2. Model simulations**

116 The National Center for Atmospheric Research (NCAR) coupled climate model, the Community Earth
117 System Model version 1.06 (CESM1.06; Hurrell et al. 2013) was used to investigate global influences of the
118 observed basin-scale ocean temperature trends for 1979–2012. This study focuses on influences of five
119 basin-scale ocean temperature: Atlantic (Atl run), IO (IO run), Pacific (Pac run), tropical Atlantic (tAtl run) and
120 tropical Pacific (tPac run; detailed below). The atmospheric component of this model is the Community
121 Atmospheric Model version 4 (CAM4; Neale et al. 2013) with F19_G16 horizontal resolution (~2°). Oceanic
122 component has ~1° horizontal resolution. The basic experimental framework of this work is generally similar to
123 Li et al. (2016). We restored basin-scale ocean mixed-layer temperature in the coupled model as follows:

124 $$F = cD\frac{T_r - T_m}{\tau}, \quad (1)$$

where c is the heat content of sea water, D is the mixed-layer depth, T_r is the restoring target temperature, T_m is the model temperature, and τ is the restoring timescale (10 days). We added external heating F to the model to restore basin-scale ocean mixed-layer temperature.

The climate response to the restored ocean mixed-layer temperature was calculated by the difference between a control run and a perturbed run. In the control run, the mixed-layer temperature was restored to the model climatology. In the perturbed run, observed temperature trend for 1979–2012 was added to the mixed-layer temperature restored in the control run. We conducted 12-member ensemble simulations with slightly different initial conditions in the control and perturbed runs. The model was integrated for 15 years and the last 10 years were used for analyses. The Atlantic, Pacific, and IO temperature were restored for the Atl, Pac and IO runs. In addition to the whole ocean basin restoring runs, we also conducted tropical-only restoring runs for the Atlantic (tAtl run) and Pacific (tPac run). In the tropical runs, the mixed-layer temperature were restored in the tropical region (20°S–20°N). Strength of temperature restoring was gradually reduced in subtropical buffer regions (30°S–20°S and 20°N–30°N).

2.3. CMIP5 multiple model ensemble

We also used the Coupled Model Intercomparison Project phase 5 (CMIP5) multiple model dataset (Taylor et al. 2012) for comparison with the CESM simulations and observations. Model data from the historical and representative concentration pathway (RCP) 4.5 runs (Meinshausen et al. 2011) were used for 1979–2005 and 2006–2012 periods, respectively. We used the results obtained from 24 models listed in Table S1 in the

online supplement. All the CMIP5 model outputs were interpolated into a 2.5° × 2.5° horizontal grid before analyses.

3. Decadal trends in summertime SST and monsoon rainfall

3.1. SST

We first examine decadal SST trends simulated in the ocean temperature restoring experiments. Physical processes associated with simulated SST due to the restored tropical ocean temperature were detailed in Li et al. (2016). Figure 1a shows observed summertime (May to September in the NH and November to March in the SH) SST trend for 1979–2012. As suggested in previous studies (e.g. Kosaka and Xie 2013; Li et al. 2016), the tropical zonally asymmetric SST trend (warming over the tropical Atlantic and IOWP and cooling over the eastern Pacific associated with positive AMO and negative PDO or IPO) is apparent. In contrast to observations, CMIP5 multi-model mean shows an overall warming without any regional cooling in the tropics (Fig. 1e), indicating the importance of natural climate variability to the observed trends (e.g. Kamae et al. 2014a, 2015). Figures 1b–d and 2 show results of the basin-scale ocean temperature restoring runs. When the North Atlantic warming is restored, the model can reproduce the general characteristics of the SST trends (i.e. the tropical zonally asymmetric SST trend; Figs. 1b, 2a; Li et al. 2016). The Gill-type atmospheric response to the tropical Atlantic warming results in surface easterly and westerly anomalies over the IO and the eastern Pacific (Fig. S5 in Li et al. 2016), leading to sea surface warming and cooling through the wind–evaporation–SST feedback (Xie and Philander 1994). In addition, the Bjerknes feedback amplifies the east–west ocean temperature asymmetry

(the western Pacific warming and the eastern Pacific cooling; Figs. 1b, 2a; Li et al. 2016). Restoring extratropical Atlantic temperature (difference between the Atl and tAtl runs) results in additional sea surface warming over the tropical western Pacific (150°E–180°; Fig. 1b) that is similar to the observations. Note that the Atl and tAtl runs do not reproduce accurately several parts of the observed SST trends (e.g. simulated cooling in the eastern tropical Pacific is weaker than the observations). Spatial coherence between the observed and simulated SST trends in the IO restoring run is limited although the western Pacific and the extratropical Atlantic warming are reproduced in this run (Fig. 1c). The Pac run cannot reproduce SST trends over the tropical Atlantic and the IO (Figs. 1d, 2b), at least in the ensemble mean. Physical mechanisms responsible for the global SST response and atmospheric circulation to the ocean temperature restoring were detailed in Li et al. (2016; see also Luo et al. 2012; Kosaka and Xie 2013; McGregor et al. 2014). Next we examine decadal trends in precipitation found in the observations and model simulations.

3.2. Global monsoon rainfall

Figures 3–5 show observed and modeled decadal precipitation trends during local summer. The observed trend since 1979 (Fig. 3a–c) exhibits regional patterns (detailed below) associated with the observed global SST trend (Fig. 1a), the AMO and PDO (e.g. Trenberth et al. 2014; Gu et al. 2016). Generally the land monsoon rainfall shows an increasing trend over the NH (Wang et al. 2013) and SH (Fig. 5a). Note that different observation datasets exhibit a large spread (Fig. 5a) particularly over the oceans (Fig. 3a–c; Wang et al. 2013, Sperber et al. 2013 Hao et al. 2016), suggesting a non-negligible observational uncertainty. Table 1 summarizes

correlation coefficients of the tropical (30°S–30°N) precipitation trends between the observations and the model simulations. The model experiments cannot reproduce accurately several parts of observed regional precipitation trends (detailed in Sects. 3.3 and 3.4), resulting in limited correlation coefficients. Generally correlations in the Atl (0.26 and 0.30 with GPCP and CMAP, respectively) and Pac (0.33 and 0.15 with GPCP and CMAP, respectively) runs are higher than the IO run and CMIP5 multi model mean (detailed below). Although the ocean temperature restoring in the Atl run is limited to the narrow area (Fig. 1), substantial remote influence on the other ocean basins and tropical land results in the high spatial correspondence of the precipitation trend. In this study, we mainly focus on land monsoon rainfall, which shows increasing trends consistently among different observational datasets except for NAF (decrease in CMAP), SAS and SAM (decrease in GPCP; Fig. 5a).

The Atl/tAtl runs can reproduce the increasing trends of NH, SH monsoons and GM rainfall (Fig. 5). The restored Atlantic temperature in these simulations contributes to the general increase in land rainfall and its spatial patterns except SAM, SAS, EAS and AUS domains (Figs. 3–5). In contrast to the Atl/tAtl runs, IO and Pac/tPac runs do not reproduce the increasing trends in GM, NH and SH rainfall (Fig. 5b). However, restored IO and Pacific Ocean temperature also lead to positive or negative trends of the regional monsoon rainfall (Fig. 5b), suggesting their partial contributions to the regional rainfall trends (detailed in Sects. 3.3 and 3.4). Here the forced response derived from the CMIP5 multi model mean shows a limited precipitation trend globally and regionally (Fig. 3g and Fig. S1 in the online supplement). Spatial correlation between the CMIP5 multi model mean and the observations is small (Table 1), indicating the importance of internal climate variability including

200 the AMO and PDO. In the later subsections, we further examine regional trends of monsoon rainfall and
201 associated physical processes.
202
203 **3.3. African and American monsoon rainfall**
204 Over tropical North Africa, the observations consistently show decreasing and increasing trends in
205 precipitation over the equator and the tropical monsoon domain (off the equator, ~10°N), respectively (Fig. 3a–c).
206 This northward shift of the precipitation band results in the increased NAF rainfall except in CMAP (Fig. 5a).
207 This increased rainfall is reproduced in the Atl/tAtl runs (Figs. 3d, 4a, 5b) but not in the IO and Pac runs.
208 The recent positive AMO-related warm tropical North Atlantic (Fig. 1) affects the position of the ITCZ
209 and strength of the NAF rainfall (Folland et al. 1986; Zhang and Delworth 2006; Ting et al. 2011;
210 Rodríguez-Fonseca et al. 2015; Kamae et al. 2016b). The IO warming in the IO run (Fig. 1) causes a reduction of
211 NAF rainfall (Figs. 3e, 5b), consistent with the suppression of tropical African rainfall by westward propagating
212 Rossby waves (Lu 2009) initiated by the IO warming (Figs. 3e, 5b; e.g. Hoerling et al. 2006). The observed
213 trends in the Pacific sea water temperature restored in the Pac/tPac runs result in reductions of NAF and SAF
214 rainfall (Figs. 3f, 4b, 5b). While previous studies emphasized the effect of the observed eastern Pacific cooling
215 on Sahel rainfall (e.g. Hoerling et al. 2006), the decreased Sahel rainfall is also affected by tropical SST
216 anomalies elsewhere (e.g. warm tropical IO). Mohino et al. (2011) showed that the tropical African rainfall
217 anomaly is quite limited if only Pacific SST anomalies are included without SST anomalies in other ocean basins
218 (Figs. 10–11 in Mohino et al. 2011). Our results suggest that the observed Pacific Ocean temperature does not

219 substantially affect SST anomalies of the tropical IO and Atlantic (Figs. 1, 2) and has a limited influence on
220 tropical African rainfall.

221 The observations show the largest increasing trends in NAM rainfall among the NH monsoons (Fig. 5a).
222 Only the Atl/tAtl runs reproduce this increasing trend quantitatively (Fig. 5b). The larger North Atlantic warming
223 compared with the South Atlantic (Fig. 1) results in an enhanced Caribbean precipitation (Figs. 3d, 4a; Ting et al.
224 2011). During the austral summer, the Atlantic warming results in an increase in near-equatorial South American
225 rainfall (contributing to an increase in SAM rainfall) and a decrease in subtropical (~20°S) South American
226 rainfall (Figs. 3d, 4a, 5b), consistent with Kushnir et al. (2010). The large and significant rainfall increases in
227 NAM, NAF and SAM in the Atl/tAtl runs contribute to the increasing trends in the NH, SH and GM rainfall (Fig.
228 5b), consistent quantitatively with the observations (0.19–0.50 mm day^{-1} 34 yr^{-1} in the observations and 0.18 ±
229 0.02, 0.19 ± 0.03 mm day^{-1} 34 yr^{-1} in the Atl and tAtl runs, respectively). In contrast, the IO run shows
230 reductions of monsoon rainfall over several domains (NAF, NAM, SAM and SAS; detailed in Sect. 3.4),
231 resulting in a suppression of GM rainfall (Fig. 5b). These negative trends suggest that the IO warming
232 compensates partly these observed positive trends. The Pacific Ocean temperature also compensates the positive
233 trends of NAM, NAF and SAF rainfall and amplifies the positive SAM rainfall trend (Fig. 5b).

234

235 **3.4. Asian and Australian monsoon rainfall**

236 The precipitation trend over the Asian monsoon regions exhibits a complex spatial pattern (Fig. 3a–c).
237 The warming trend over the IOWP (Fig. 1a; Solomon and Newman 2012; Roxy et al. 2014) induces a local

238 increase in precipitation over the ocean (Fig. 3a, b; Zhou et al. 2009; Wang et al. 2012; Ueda et al. 2015).
239 Summertime precipitation is suppressed over the central-east and northern regions of the Indian subcontinent and
240 is increased over the southwestern regions (Figs. 3a–d, 4a) associated with the tropical (the Atlantic and IOWP)
241 oceanic warming (Figs. 1a, b, 2a; Mishra et al. 2012; Roxy et al. 2015). These regional variations in precipitation
242 trends are reproduced in the Atl/tAtl runs (Figs. 3d, 4a). Over the SAS and EAS domains, the observed land
243 monsoon rainfall shows generally positive trends (not statistically significant in GPCP; Figs. 3a, 5a). The
244 Atl/tAtl runs do not show systematic trends over the SAS and EAS domains (Figs. 3d, 5b), suggesting a limited
245 contribution of the Atlantic Ocean to the rainfall trends over the Asian land monsoon domains.

246 Atlantic temperature influences on Indian monsoon rainfall through the shift of ITCZ, Eurasian
247 continental warming and mid-latitude wavetrain (Goswami et al. 2006; Li et al. 2008; Wang Y et al. 2009; Ting
248 et al. 2011). Zhang and Delworth (2006) reported a relationship between the North Atlantic warming and the
249 increased Indian rainfall, which is not apparent in our simulations (Figs. 3d, 4a). The Atlantic warming also
250 results in an IO warming (Fig. 1b) through eastward propagating Kelvin wave (Kucharski et al. 2009; Wang C et
251 al. 2009; Li et al. 2016). Here the IO warming restored in the IO run and Eurasian warming produces the
252 opposite effects on the Asian monsoon via changing MTG (Zuo et al. 2013). The IO warming also leads to an
253 enhanced water vapor advection that can increase South Asian monsoon rainfall (Roxy et al. 2015; Ueda et al.
254 2015). Section 4 further examines the competition between the IO and Eurasian continental warming in the MTG
255 and the Asian monsoon.

256 The Pac/tPac runs with eastern-cool/western-warm SST anomaly over the tropical Pacific simulate the
257 increased western North Pacific and SAS rainfall (Figs. 3f, 4b, 5). The relationship between the Pacific zonally
258 asymmetric SST anomaly and the Indian rainfall is consistent with previous reports (Rasmusson and Carpenter
259 1983; Webster and Yang 1992; Kawamura 1998; Kumar et al. 1999; Mishra et al. 2012). However, the
260 contributions of the Pac/tPac to NAM, NAF, SAM, and SAF rainfall are limited (Figs. 3f, 4b, 5b), resulting in an
261 inconsistent trend of GM rainfall with the observations (Fig. 5). The IO warming restored in the IO run causes to
262 increase the local rainfall (Fig. 3e; Xie et al. 2009; Ueda et al. 2015) but suppresses rainfall over the interior of
263 the Indian subcontinent via reducing MTG between the Asian continent and the tropical ocean (Fig. 3e; see Sect.
264 4; Mishra et al. 2012; Roxy et al. 2015). In short, the general reduction of land monsoon rainfall simulated in the
265 IO run (Figs. 3e, 5b) can largely be explained by the suppression of interior continental rainfall over India,
266 reduction of adjacent tropical African rainfall (Hoerling et al. 2006), and reduced NAM and SAM rainfall. The
267 increase in SAS rainfall in the Pac run is larger than the Atl run (Fig. 5b), consistent with differences in the
268 simulated SST between the two runs (the weakened eastern Pacific cooling and warmed IO in the Atl run; Fig.
269 1).

270 All the observation datasets exhibit substantial increasing trend in the AUS rainfall (1.2–1.4 mm day^{-1} 34
271 yr^{-1}; Fig. 5a). None of the experiments reproduce the AUS rainfall increase (Figs. 3, 4, 5b) despite strong
272 controls of the IO and Pacific SST anomalies on northern Australian rainfall (e.g. Cai and van Rensch 2013).
273 Rotstayn et al. (2007) pointed out that aerosols are essential factors for the observed increasing trend of

summertime rainfall over northwestern Australia (Smith 2004; Taschetto and England 2009) since the late 20th century. The aerosols effect is not explicitly included in our simulation, where aerosols are held constant in time.

4. Meridional thermal gradient and global monsoon

Variations in the horizontal temperature gradient are suggested to be important for interpretation of large-scale variations in the monsoon strength on different timescales: seasonal to interannual (Li and Yanai 1996; Kawamura 1998), decadal (Zuo et al. 2013), and centennial to millennium (Ueda et al. 2006, 2011; Man et al. 2012; Zuo et al. 2013; Roxy et al. 2015; Mohtadi et al. 2016). In this section, we advance our interpretation on dynamic and thermodynamic properties of the recent decadal GM trend. Figure 6a shows climatologies of mid-to-upper tropospheric thickness (between 200 and 500 hPa levels) and vertical wind shear between lower and upper troposphere (850 hPa minus 200 hPa). Horizontal gradient of climatological thickness corresponds to deep tropospheric temperature gradient. Through a thermal wind balance, variation in the thickness corresponds well with an index for seasonal cycle and interannual variability of the South Asian monsoon (Webster-Yang index) determined by the tropospheric wind shear (Webster and Yang 1992). The tropospheric thickness and vertical wind shear can explain changes in atmospheric thermodynamic structure and atmospheric stability in a perturbed climate (Ma et al. 2012; Kamae et al. 2016a). Thick lines in Fig. 6a indicate latitudes with peak thickness in each hemisphere. Peak latitudes over longitudinal areas with continents (and associated monsoon systems) are displaced from the equator. Here monsoonal circulations are formed along with resultant meridional peak-to-equator thickness gradient (i.e. MTG). Over South Asia, the peak latitude is farthest from the equator,

293 the peak thickness (i.e. the South Asian High) is largest and the Asian monsoon is strongest over the globe (e.g.
294 Li and Yanai 1996). The peak latitude is located on the equator over longitudinal areas without any monsoon
295 systems (e.g. the central Pacific).

296 Figure 6b shows trends of the thickness and wind shear for 1979–2012 derived from the reanalysis. A
297 recent trend in the mid-to-upper tropospheric thickness can be characterized by increases over subtropical
298 continents (Fig. 6b) and decreases over the tropical central-to-eastern Pacific associated with the tropical Pacific
299 cooling (Kamae et al. 2015). Vertical wind shear (low-level westerly and upper-level easterly) is strengthened
300 over the tropical NH (0°N–15°N; Wang et al. 2013), corresponding to the positive MTG trend (Fig. 6b). We can
301 examine trends of the monsoon strength by comparing the thickness trends on the climatological peak latitude
302 (dashed line in Fig. 6b) and the equator (detailed below). Most parts of the subtropics except the western Pacific
303 exhibit larger positive thickness trend than the equator, indicating enhanced MTG. This positive MTG trend can
304 explain well the trend in wind shear (Fig. 6b). Here the increasing trends in MTG and wind shear are consistent
305 with the positive trend in the monsoon rainfall (Fig. 5).

306 Figures 6c–e and 7 show results of the individual ocean temperature restoring runs. The Atl/tAtl runs
307 reproduce the GM rainfall increase with the subtropical peaks of thickness trends over the North and South
308 Atlantic and South IO. Figure 8 shows MTG trends as represented by the difference in thickness trends over the
309 peak latitude (black line in Fig. 6) and the equator. The observed MTG trends are positive except 100°E–160°E
310 in the NH and except 140°E–180°E in the SH, generally consistent with the positive trend in GM rainfall (Fig. 5).
311 The Atl/tAtl runs reproduce warming trends over the tropical Atlantic and IOWP (Figs. 1b, 2a) and associated

312 regional tropospheric warming (Figs. 6c, 7a). For example, the recent tropical Atlantic warming favors an
313 eastward propagating Kelvin wave and subtropical westward propagating Rossby waves (Kamae et al. 2014a; Li
314 et al. 2016), resulting in (1) the positive thickness trends over subtropical North and South America, North and
315 South Atlantic, and North Africa; and (2) the positive thickness trends over the tropical IO (Figs. 6c, 7a)
316 associated with the IO warming (Figs. 1b, 2a) through a wind–evaporation–SST feedback (i.e. reduced scalar
317 wind speed over the tropical IO results in sea surface warming; Xie and Philander 1994; Li et al. 2016). The
318 Atl/tAtl runs reproduce the NH and SH subtropical peaks of the thickness trends over the Atlantic (Figs. 6c, 7a)
319 and the positive MTG trend from the Western Hemisphere to 50°E (Fig. 8a). Note that the simulated trends over
320 the SH are not statistically significant and are smaller than the observations (Fig. 8b).

321 The tAtl run simulates the recent trends in the MTG and the wind shear, similar to the Atl run, indicating
322 an importance of the tropical Atlantic temperature trend in the dynamic and thermodynamic aspects of the recent
323 GM enhancement (Figs. 7a, 8). The extratropical North Atlantic warming is absent in the tAtl run (Fig. 2a),
324 leading to differential tropospheric warming over the NH extratropics including North Africa and Eurasian
325 continent (Fig. 7a; e.g. Lu et al. 2006; Wang Y et al. 2009; Zuo et al. 2013) and resultant MTG trend over 10°W–
326 140°E (Fig. 8a; negative and positive in the tAtl and Atl runs, respectively). This result is qualitatively consistent
327 with the difference in precipitation trends over NAF and SAS domains between the two runs (larger in the Atl
328 run than the tAtl run; Fig. 5b).

329 The Atl/tAtl runs exhibit different MTG trends to the observations over the SAS domain (Figs. 6, 8a). The
330 observed thickness trend over West, South and East Asia exhibit a wavy pattern (Fig. 6b), suggesting an

importance of mid-latitude atmospheric internal variability (e.g. Kamae et al. 2014a, 2016b). In the Atl run, the Eurasian warming is underestimated (Fig. 6c) and associated MTG trend is opposite to the observations (Fig. 8a) although SST warming over the North Atlantic and tropical IO are reproduced well (Fig. 1). Similarly, the Atl run exhibits an opposite trend in atmospheric circulation (easterly shear; Fig. 6c) to the observation (westerly shear; Fig. 6b) over the tropical IOWP (EQ–15°N; 50°E–130°E). These results are consistent with different land precipitation trends over South Asia between the Atl run and the observations (Figs. 3d, 5b). In contrast, the Pac/tPac runs exhibit larger thickness trend over the Eurasian continent than over the tropical IO, intensifying the Asian monsoon circulation and SAS rainfall (Figs. 3f, 4b, 5b, 6e, 8b). These results indicate that the trans-basin teleconnection initiated by the Atlantic Ocean contributes to the recent intensification of GM but cannot explain some of the observed trends including those over the SAS. In the SH, the Atlantic temperature also contributes to the enhanced SAM through the tropical warming (Figs. 5b, 6c, 7a, 8) but cannot explain generally the recent AUS rainfall increase, to which aerosols might be important (Rotstayn et al. 2007; see Sect. 3.4).

5. Summary and discussion

We systematically examine contributions of large-scale decadal climate variability to the recent enhancement of GM from a dynamic-thermodynamic perspective. The North Atlantic warming contributes to the regional patterns of SST trend over the tropics and associated increasing trend of GM rainfall through the trans-basin atmosphere–ocean interactions. The warm tropical Atlantic reinforces the monsoon circulations and rainfall over NAM, SAM and NAF domains. In addition, the extratropical North Atlantic warming contributes to

350 the increasing trend of MTG over South Asia via Eurasian continental warming, but it cannot explain the
351 increased SAS rainfall quantitatively. The increased AUS rainfall cannot be reproduced by any of the ocean
352 temperature restoring experiments conducted in the current study, supporting the hypothesis that anthropogenic
353 aerosols are essential for the recent increasing trend in AUS rainfall. The great importance of the
354 Atlantic-induced pan-tropical decadal variability in the GM system suggests a possible weakening of the GM in
355 accordance with a phase shift of the Atlantic multidecadal variability mode in the near future.

356 The results of this study indicate the great contribution of the Atlantic warming to the several aspects of
357 the recent decadal climate trends including monsoons. However, the Atlantic temperature restoring experiment
358 performed in this study cannot reproduce parts of the observed SST trends. For example, SST trends over the
359 eastern tropical and subtropical Pacific (cooling over the tropics and warming over the middle latitude) are
360 generally underestimated (Fig. 1a, b). Such regional differences in SST trends compared with the observations
361 possibly affect land monsoon rainfall via large-scale atmospheric teleconnections (e.g. Pacific-North American
362 pattern; Mo and Livezey 1986) and atmospheric thermodynamic structure (Fig. 6). We should also keep in mind
363 that the AOGCM is not necessarily perfect in simulating trends of atmospheric circulation and precipitation even
364 if the AOGCM can simulate accurately the global SST trends. Additional experiments including global ocean
365 temperature restoring experiment may be effective to separate effects of the regional SST biases, model's own
366 biases, and the missing external forcing agents (i.e. aerosols). It is also needed to compare the results of this
367 study with similar restoring experiments performed by other AOGCMs to address robustness of the results.

Future modeling efforts by multiple climate models may improve our understanding of importance of the trans-basin atmosphere–ocean interactions in the trends of global climate system including monsoons.

Via restoring ocean temperature, Wang et al. (2013) also pointed out the importance of the North Atlantic warming in the recent intensification of the NH monsoons. The current study provides a more comprehensive view on the individual basin-scale ocean temperature contributions to the GM trend. The use of MTG can offers a physical interpretation of decadal variabilities of the global and regional monsoons. The recent regional MTG trends correspond well to the summertime precipitation trends for the last 34 years. We should note that MTG is not necessarily a universal index for long-term rainfall change due to an importance of thermodynamic rainfall change in a warming climate despite the robust dynamic rainfall change (e.g. Ueda et al. 2006; Endo and Kitoh 2014). Further research into monsoon variability and changes helps advance predictive understanding of changes in global atmospheric circulation and associated regional climate change (Xie et al. 2015).

Acknowledgements

The authors are grateful to two anonymous reviewers for their constructive comments. We acknowledge the World Climate Research Programme's Working Group on Coupled Modeling, which is responsible for CMIP, and we thank the climate modeling groups (listed in Table S1 in the online supplement) for producing and making available their model output. For CMIP5, the US Department of Energy's Program for Climate Model Diagnosis and Intercomparison provided coordinating support, and led the development of the software infrastructure in partnership with the Global Organization for Earth System Science Portals.

387

388 **References**

389 An Z et al (2015) Global monsoon dynamics and climate change. Ann Rev Earth Planet Sci 43:29–77.
390 doi:10.1146/annurev-earth-060313-054623

391 Arai M, Kimoto M (2008) Simulated interannual variation in summertime atmospheric circulation associated
392 with the East Asian monsoon. Clim Dyn 31:435–447

393 Bollasina MA, Ming Y, Ramaswamy V (2011) Anthropogenic aerosols and the weakening of the south Asian
394 summer monsoon. Science 334:502–505

395 Cai W, van Rensch P (2013) Austral summer teleconnections of Indo-Pacific variability: their nonlinearity and
396 impacts on Australian climate. J Clim 26:2796–2810

397 Chikamoto Y et al. (2015) Skilful multi-year predictions of tropical trans-basin climate variability. Nature Comm
398 6:6869. doi:10.1038/ncomms7869

399 Christensen JH, Krishna Kumar K, Aldrian E et al (2014) Climate phenomena and their relevance for future
400 regional climate change. In: Stocker TF, editor. Climate change 2013: the physical science basis.
401 Contribution of working group I to the Fifth Assessment Report of the Intergovernmental Panel on Climate
402 Change. Cambridge, Cambridge University Press p. 1217–1308

403 Dai A, Li H, Sun Y, Hong L-C, LinHo, Chou C, Zhou T (2013) The relative roles of upper and lower
404 tropospheric thermal contrasts and tropical influences in driving Asian summer monsoons. J Geophys Res
405 Atmos 118:7024–7045

406 Dee DP et al (2011) The ERA-Interim reanalysis: configuration and performance of the data assimilation system.
407 Q J Roy Meteorol Soc 137:553–597

408 Deser C, Phillips AS, Hurrell JW (2004) Pacific interdecadal climate variability: linkages between the tropics
409 and the North Pacific during boreal winter since 1900. J Clim 17:3109–3124

410 Dong B, Sutton RT, Highwood EJ, Wilcox LJ (2016) Preferred response of the East Asian summer monsoon to
411 local and non-local anthropogenic sulphur dioxide emissions. Clim Dyn 46: 1733–1751

412 Endo H, Kitoh A (2014) Thermodynamic and dynamic effects on regional monsoon rainfall changes in a warmer
413 climate. Geophys Res Lett 41:1704–1710. doi:10.1002/2013gl059158

414 Folland CK, Palmer TN, Parker DE (1986) Sahel rainfall and worldwide sea temperatures, 1901–85. Nature
415 320:602–607

416 Goswami BN, Madhusoodanan M, Neema C, Sengupta D (2006) A physical mechanism for North Atlantic SST
417 influence on the Indian summer monsoon. Geophys Res Lett 33:L02706. doi:10.1029/2005GL024803

418 Gu F, Adler RF, Huffman GJ (2016) Long-term changes/trends in surface temperature and precipitation during
419 the satellite era (1979–2012). Clim Dyn 46:1091–1105

Harris I, Jones PD, Osborn TJ, Lister DH (2014) Updated high-resolution grids of monthly climatic observations – the CRU TS3.10 Dataset. Int J Climatol 34:623–642

Hao Y-Q, Zhu C-W, Liu B-Q (2016) Discrepancies in boreal summer monsoon rainfall between GPCP and CMAP products during 1979–2014. Atmos Ocean Sci Lett 9:226–233

Hoerling M, Hurrell J, Eischeid J, Phillips A (2006) Detection and attribution of 20th century northern and southern African rainfall change. J Clim 19:3989–4008

Hsu P-C, Li T, Wang B (2011) Trends in global monsoon area and precipitation over the past 30 years. Geophys Res Lett 38:L08701. doi:10.1029/2011GL046893

Hsu P-C, Li T, Luo J-J, Murakami H, Kitoh A, Zhao M (2012) Increase of global monsoon area and precipitation under global warming: A robust signal? Geophys Res Lett 39:L06701. doi:10.1029/2012GL051037

Hsu P-C, Li T, Murakami H, Kitoh A (2013) Future change of the global monsoon revealed from 19 CMIP5 models. J Geophys Res Atmos 118:1247–1260

Hurrell JW et al (2013) The Community Earth System Model: A framework for collaborative research. Bull Am Meteorol Soc 94:1339–1360

Huffman GJ, Adler RF, Bolvin DT, Gu G (2009) Improving the global precipitation record: GPCP Version 2.1. Geophys Res Lett 36:L17808. doi:10.1029/2009GL040000

Hwang Y-T, Frierson DMW, Kang SM (2013) Anthropogenic sulfate aerosol and the southward shift of tropical precipitation in the late 20th century. Geophys Res Lett 40:2845–2850

Jiang D, Tian Z, Lang X, Kageyama M, Ramstein G (2015) The concept of global monsoon applied to the last glacial maximum: A multi-model analysis. Quat Sci Rev 126:126–139

Kamae Y, Shiogama H, Watanabe M, Kimoto M (2014a) Attributing the increase in Northern Hemisphere hot summers since the late 20th century. Geophys Res Lett 41:5192–5199

Kamae Y, Watanabe M, Kimoto M, Shiogama H (2014b) Summertime land–sea thermal contrast and atmospheric circulation over East Asia in a warming climate–Part I: Past changes and future projections. Clim Dyn 43:2553–2568

Kamae Y, Shiogama H, Watanabe M, Ishii M, Ueda H, Kimoto M (2015) Recent slowdown of tropical upper tropospheric warming associated with Pacific climate variability. Geophys Res Lett 42:2995–3003

Kamae Y, Ogura T, Watanabe M, Xie S-P, Ueda H (2016a) Robust cloud feedback over tropical land in a warming climate. J Geophys Res Atmos 121:2593–2609

Kamae Y et al (2016b) Forced response and internal variability of summer climate over western North America. Clim Dyn. doi:10.1007/s00382-016-3350-x

Kawamura R (1998) A possible mechanism of the Asian summer monsoon-ENSO coupling. J Meteorol Soc Jpn 76:1009–1027

Kawase H, Takemura T, Nozawa T (2011) Impact of carbonaceous aerosols on precipitation in tropical Africa during the austral summer in the twentieth century. J Geophys Res 116:D18116. doi:10.1029/2011JD015933

Kitoh A, Endo H, Krishna Kumar K, Cavalcanti IFA, Goswami P, Zhou T (2013) Monsoons in a changing world: A regional perspective in a global context. J Geophys Res Atmos 118:3053–3065

Kosaka Y, Xie S-P (2013) Recent global-warming hiatus tied to equatorial Pacific surface cooling. Nature 501:403–407

Kucharski F, Bracco A, Yoo JH, Tompkins A, Feudale L, Ruti P, Dell'Aquila A (2009) A Gill-Matsun-type mechanism explains the Tropical Atlantic influence on African and Indian Monsoon rainfall. Quart J R Met Soc 135:569–579

Kucharski F et al (2016) Atlantic forcing of Pacific decadal variability. Clim Dyn 46: 2337–2351

Kumar KK, Rajagopalan B, Cane MA (1999) On the weakening relationship between the Indian monsoon and ENSO. Science 284:2156–2159

Kushnir Y, Seager R, Ting MF, Naik N, Nakamura J (2010) Mechanisms of tropical Atlantic SST influence on North American precipitation variability. J Clim 23:5610–5628

Lee J-Y, Wang B (2014) Future change of global monsoon in the CMIP5. Clim Dyn 42:101–119

Li CF, Yanai M (1996) The onset and interannual variability of the Asian summer monsoon in relation to land-sea thermal contrast. J Clim 9:358–375

Li S, Perlwitz J, Quan X, Hoerling MP (2008) Modelling the influence of North Atlantic multidecadal warmth on the Indian summer rainfall. Geophys Res Lett 35:L05804. doi:10.1029/2007GL032901

Li X, Xie S-P, Gille ST, Yoo C (2016) Atlantic-induced pan-tropical climate change over the past three decades. Nature Clim Change 6:275–279

Lin R, Zhou T, Qian Y (2014) Evaluation of global monsoon precipitation changes based on five reanalysis datasets. J Clim 27:1271–1289

Lu J (2009) The dynamics of the Indian Ocean sea surface temperature forcing of Sahel drought. Clim Dyn 33: 445–460

Lu R, Dong B, Ding H (2006) Impact of the Atlantic Multidecadal Oscillation on the Asian summer monsoon. Geophys Res Lett 33:L24701. doi:10.1029/2006GL027655

Luo JJ, Sasaki W, Masumoto Y (2012) Indian Ocean warming modulates Pacific climate change. Proc Natl Acad Sci USA 109:18701–18706

Ma J, Yu J-Y (2014) Paradox in South Asian summer monsoon circulation change: Lower tropospheric strengthening and upper tropospheric weakening. Geophys Res Lett 41:2934–2940

Ma J, Xie S-P, Kosaka Y (2012) Mechanisms for tropical tropospheric circulation change in response to global warming. J Clim 25:2979–2994

Man W, Zhou T, Jungclaus JH (2012) Simulation of the East Asian summer monsoon during the last millennium with the MPI earth system model. J Clim 25:7852–7866

McGregor S et al (2014) Recent Walker circulation strengthening and Pacific cooling amplified by Atlantic warming. Nature Clim Change 4:888–892

Meinshausen M et al (2011) The RCP greenhouse gas concentrations and their extensions from 1765 to 2300. Clim Change 109:213–241

Mishra V, Smoliak BV, Lettenmaier DP, Wallace JM (2012) A prominent pattern of year-to-year variability in Indian Summer Monsoon Rainfall. Proc Natl Acad Sci USA 109:7213–7217

Mo KC, Livezey RE (1986) Tropical–extratropical geopotential height teleconnections during the Northern Hemisphere winter. Mon Weather Rev 114:2488–2515

Mohino E, Janicot S, Bader J (2011) Sahel rainfall and decadal to multi-decadal sea surface temperature variability Clim Dyn (2011) 37:419–440

Mohtadi M, Prange M, Steinke S (2016) Palaeoclimatic insights into forcing and response of monsoon rainfall. Nature 533:191–199

Murakami T, Matsumoto J (1994) Summer monsoon over the Asian continent and western North Pacific. J Meteorol Soc Jpn 72:719–745

Neale RB, Richter J, Park S, Lauritzen PH, Vavrus SJ, Rasch PJ, Zhang M (2013) The mean climate of the Community Atmosphere Model (CAM4) in forced SST and fully coupled experiments. J Clim 26:5150–5168

Newman M et al (2016) The Pacific Decadal Oscillation, revisited. J Clim 29:4399–4427

Ogata T et al (2014) Projected future changes in the Asian Monsoon: A comparison of CMIP3 and CMIP5 model results. J Meteorol Soc Jpn 92:207–225

Polson D, Bollasina M, Hegerl GC, Wilcox LJ (2014) Decreased monsoon precipitation in the Northern Hemisphere due to anthropogenic aerosols. Geophys Res Lett 41:6023–6029

Power S, Casey T, Folland C, Colman A, Mehta V (1999) Interdecadal modulation of the impact of ENSO on Australia. Clim Dyn 15:319–324

Rasmusson EM, Carpenter TH (1983) Relationship between eastern equatorial Pacific sea surface temperatures and rainfall over India and Sri Lanka. Mon Weather Rev 111:517–528

Rayner NA et al (2003) Global analyses of sea surface temperature, sea ice, and night marine air temperature since the late nineteenth century. J Geophys Res 108(D14):4407. doi:10.1029/2002JD002670

Rodríguez-Fonseca B et al (2015) Variability and predictability of West African droughts: a review on the role of sea surface temperature anomalies. J Clim 28:4034–4060

Rotstayn LD, Lohmann U (2002) Tropical rainfall trends and the indirect aerosol effect. J Clim 15:2103– 2116

519 Rotstayn LD, Ryan BF, Penner JE (2000) Precipitation changes in a GCM resulting from the indirect effects of
520 anthropogenic aerosols. Geophys Res Lett 27:3045–3048

521 Rotstayn LD et al (2007) Have Australian rainfall and cloudiness increased due to the remote effects of Asian
522 anthropogenic aerosols? J Geophys Res 112:D09202. doi:10.1029/2006JD007712

523 Roxy MK, Ritika K, Terray P, Masson S (2014) The curious case of Indian Ocean warming. J Clim 27:8501–
524 8509

525 Roxy MK, Ritika K, Terray P, Murtugudde R, Ashok K, Goswami BN (2015) Drying of Indian subcontinent by
526 rapid Indian Ocean warming and a weakening land-sea thermal gradient. Nature Communications 6:7423.
527 doi:10.1038/ncomms8423

528 Smith IN (2004) An assessment of recent trends in Australian rainfall. Aust Meteor Mag 53:163–173

529 Solomon A, Newman M (2012) Reconciling disparate twentieth-century Indo-Pacific ocean temperature trends
530 in the instrumental record. Nature Clim Change 2:691–699

531 Sooraj KP, Terray P, Mujumdar M (2015) Global warming and the weakening of the Asian summer monsoon
532 circulation: assessments from the CMIP5 models. Clim Dyn 45:233–252

533 Sperber KR, Annamalai H, Kang I-S, Kitoh A, Moise A, Turner A, Wang B, Zhou T (2013) The Asian summer
534 monsoon: an intercomparison of CMIP5 vs. CMIP3 simulations of the late 20th century. Clim Dyn 41:2711–
535 2744

536 Stevens B and Feingold G (2009) Untangling aerosol effects on clouds and precipitation in a buffered system.
537 Nature 461:607–613

538 Sun Y, Ding Y, Dai A (2010) Changing links between South Asian summer monsoon circulation and tropospheric
539 land-sea thermal contrasts under a warming scenario. Geophys Res Lett 37:L02704.
540 doi:10.1029/2009GL041662

541 Taschetto AS and England MH (2009) An analysis of late 20th century trends in Australian rainfall. Int J
542 Climatol 29:791–807

543 Taylor KE, Stouffer RJ, Meehl GA (2012) An overview of CMIP5 and the experiment design. Bull Am Meteorol
544 Soc 90:485–498

545 Terray P, Masson S, Prodhomme C, Roxy MK, Sooraj KP (2016) Impacts of Indian and Atlantic oceans on
546 ENSO in a comprehensive modeling framework. Clim Dyn 46:2507–2533

547 Ting M, Kushnir Y, Seager R, Li C (2011) Robust features of Atlantic multi-decadal variability and its climate
548 impacts. Geophys Res Lett 38:L17705. doi:10.1029/2011GL048712

549 Trenberth KE, Stepaniak DP, Caron JM (2000) The Global monsoon as seen through the divergent atmospheric
550 circulation. J Clim 13:3969–3993

551 Trenberth KE, Fasullo JT, Branstator G, Phillips S (2014) Seasonal aspects of the recent pause in surface
552 warming. Nature Clim Change 4:911–916

553 Ueda H, Iwai A, Kuwako K, Hori ME (2006) Impact of anthropogenic forcing on the Asian summer monsoon as
554 simulated by 8 GCMs. Geophys Res Lett 33:L06703. doi:10.1029/2005GL025336

555 Ueda H, Kuroki H, Ohba M, Kamae Y (2011) Seasonally asymmetric transition of the Asian monsoon in
556 response to ice age boundary conditions. Clim Dyn 37:2167–2179

557 Ueda H, Kamae Y, Hayasaki M, Kitoh A, Watanabe A, Miki Y, Kumai A (2015) Combined effects of recent
558 Pacific cooling and Indian Ocean warming on the Asian monsoon. Nature Communications 6:8854. doi:
559 10.1038/ncomms9854

560 Wang B, Ding QH (2006) Changes in global monsoon precipitation over the past 56 years. Geophys Res Lett
561 33:L06711. doi:10.1029/2005GL025347

562 Wang B, Ding QH (2008) Global monsoon: dominant mode of annual variation in the tropics. Dyn Atmos
563 Oceans 44:165–183

564 Wang B, Ding Q, Fu Z, Kang I-S, Jin K, Shukla J, Doblas-Reyes F (2005) Fundamental challenge in simulation
565 and prediction of summer monsoon rainfall. Geophys Res Lett 32:L15711. doi:10.1029/2005GL022734

566 Wang B, Liu J, Kim HJ, Webster PJ, Yim SY (2012) Recent change of the global monsoon precipitation (1979–
567 2008). Clim Dyn 39:1123–1135

568 Wang B, Liu J, Kim HJ, Webster PJ, Yim SY, Xiang B (2013) Northern Hemisphere summer monsoon
569 intensified by mega-El Nino/southern oscillation and Atlantic multidecadal oscillation. Proc Natl Acad Sci
570 USA 110:5347–5352

571 Wang C, Kucharski F, Barimalala R, Bracco A (2009) Teleconnections of the tropical Atlantic to the tropical
572 Indian and Pacific Oceans: A review of recent findings. Meteorol Zeitschr 18: 445–454

573 Wang H, Xie S-P, Liu Q (2016) Comparison of climate response to anthropogenic aerosol versus greenhouse gas
574 forcing: distinct patterns. J Clim 29:5205–5222

575 Wang PX, Wang B, Cheng H, Fasullo J, Guo ZT, Kiefer T, Liu ZY (2014) The global monsoon across
576 timescales: coherent variability of regional monsoons. Clim Past 10:2007–2052

577 Wang Y, Li S, Luo D (2009) Seasonal response of Asian monsoonal climate to the Atlantic Multidecadal
578 Oscillation. J Geophys Res 114:D02112. doi:10.1029/2008JD010929

579 Watanabe M, Kamae Y, Yoshimori M, Oka A, Sato M, Ishii M, Mochizuki T, Kimoto M (2013) Strengthening of
580 ocean heat uptake efficiency associated with the recent climate hiatus. Geophys Res Lett 40:3175–3179

581 Watanabe M, Shiogama H, Tatebe H, Hayashi M, Ishii M, Kimoto M (2014) Contribution of natural decadal
582 variability to global-warming acceleration and hiatus. Nature Clim Change 4:893–897

583 Webster PJ (2006) The development of a holistic view of the monsoon. In: Wang B (ed) The Asian monsoon.
584 Springer/Praxis Publishing Co., New York, p 787

585 Webster PJ, Yang S (1992) Monsoon and ENSO: Selectively interactive systems. Quart J Roy Meteorol Soc
586 118:877–926

Webster PJ et al (1998) Monsoons: Processes, predictability, and the prospects for prediction. J Geophys Res 103(C7):14451–14510

Xie P, Arkin PA (1997) Global Precipitation: A 17-year monthly analysis based on gauge observations, satellite estimates, and numerical model outputs. Bull Am Meteorol Soc 78:2539–2558

Xie S-P, Philander SGH (1994) A coupled ocean-atmosphere model of relevance to the ITCZ in the eastern Pacific. Tellus A 46:340–350

Xie S-P et al (2009) Indian Ocean capacitor effect on Indo–Western Pacific climate during the summer following El Niño. J Clim 22:730–747

Xie S-P et al (2015) Towards predictive understanding of regional climate change. Nature Clim Change 5:921–930

Yan M, Wang B, Liu J (2016) Global monsoon change during the Last Glacial Maximum: a multi-model study. Clim Dyn 47: 359–374

Zhang R, Delworth TL (2006) Impact of Atlantic multidecadal oscillations on India/Sahel rainfall and Atlantic hurricanes. Geophys Res Lett 33:L17712. doi:10.1029/2006GL026267

Zhou T et al (2009) Why the Western Pacific Subtropical High has extended westward since the late 1970s. J Clim 22:2199–2215

Zuo Z, Yang S, Zhang R, Jiang P, Zhang L, Wang F (2013) Long-term variations of broad-scale Asian Summer Monsoon circulation and possible causes. J Clim 26:8947–8961

607 **Table captions**

608

609 **Table 1.** Correlation coefficients for decadal precipitation trend for 1979–2012 over the tropics (30°S–30°N)

610 between observations and model simulations

611

612 **Figure captions**

613

614 **Fig. 1** Decadal trends in summertime sea surface temperature (SST; K 34 yr^{-1}) for 1979–2012. Averages for May
615 to September and November to March are shown in the Northern and Southern Hemispheres, respectively.
616 Three-year running means are applied before calculating linear trends. (a) Observed trend in HadISST. (b)
617 12-member ensemble means of Atl, (c) IO, and (d) Pac runs, respectively. (e) CMIP5 24-model ensemble
618 mean. Models used are listed in Table S1 in the online supplement

619

620 **Fig. 2** Similar to Fig. 1b–d but for (a) tAtl and (b) tPac runs, respectively

621

622 **Fig. 3** Similar to Fig. 1 but for summertime precipitation (mm day^{-1} $34yr^{-1}$). (a) Observed trends in GPCP, (b)
623 CMAP, and (c) CRU TS v3.23. Stipples indicate areas with trends that are significant at the 95 % confidence
624 level or higher. Areas surrounded by purple lines indicate land monsoon domains (North American
625 Monsoon; NAM, South American Monsoon; SAM, North African Monsoon; NAM, South African
626 Monsoon; SAM, South Asian Monsoon; SAM, East Asian Monsoon; EAM, Australian Monsoon; AUS). (d)
627 Results of Atl, (e) IO, and (f) Pac runs, respectively. (g) 24-model mean of the CMIP5 multiple model
628 ensemble

629

630 **Fig. 4** Similar to Fig. 2d–f but for (a) tAtl and (b) tPac runs, respectively

631

632 **Fig. 5** Decadal trends in summertime precipitation (mm day^{-1} $34yr^{-1}$) averaged over the global land monsoon
633 domain (GM), Northern and Southern Hemisphere monsoon domains (NH and SH), and individual monsoon
634 domains (purple areas shown in Fig. 3). (a) Observed trends in CRU TS v3.23 (grey bar with solid line),
635 GPCP (dotted line) and CMAP (dashed line). Three error bars indicate 95% confidence intervals for (left to
636 right) CRU, GPCP and CMAP, respectively. (b) Modeled trends in Atl (blue bar), IO (orange bar) and Pac
637 (red bar) runs. Black rectangles represent results of tAtl and tPac runs. Error bars indicate 95% confidence
638 intervals. Grey and black error bars on the blue (red) bars indicate Atl and tAtl (Pac and tPac) runs,
639 respectively. Solid, dotted and dashed grey rectangles are identical to (a)

640

641 **Fig. 6** Summertime mid-to-upper tropospheric thickness (Z200 minus Z500; shading; m) and vertical wind shear
642 (850 hPa minus 200 hPa; vector; m s^{-1}). (a) Climatology for 1979–2012 in ERA-Interim. Thick black lines
643 indicate latitudes with peak thickness in the individual hemispheres. (b) Decadal trend for 1979–2012 in
644 ERA-Interim. Dashed lines represent the peak thickness in climatology, identical to the solid lines in (a). (c)
645 Results of Atl, (d) IO, and (e) Pac runs, respectively

646

647 **Fig. 7** Similar to Fig. 6c–e but for (a) tAtl and (b) tPac runs, respectively

Fig. 8 Difference in decadal trends of summertime mid-to-upper tropospheric thickness (Z200 minus Z500) for 1979–2012 (m $34yr^{-1}$) between the peak latitude (black line in Fig. 6) and the equator. (a) ERA-Interim (grey), Atl (blue), IO (orange), and Pac (red) runs over the Northern and (b) Southern Hemispheres, respectively. Shadings represent 95% confidence intervals. Dashed blue and red lines indicate tAtl and tPac runs, respectively. Black lines in the lower parts represent longitudinal areas of the land monsoon domains

655 **Table 1.** Correlation coefficients for decadal precipitation trend for 1979–2012 over the tropics (30°S–30°N)

656 between observations and model simulations

Experiments	GPCP	CMAP
Atl	0.26	0.30
IO	0.11	–0.02
Pac	0.33	0.15
tAtl	0.26	0.27
tPac	0.32	0.14
CMIP5	0.24	–0.10

657

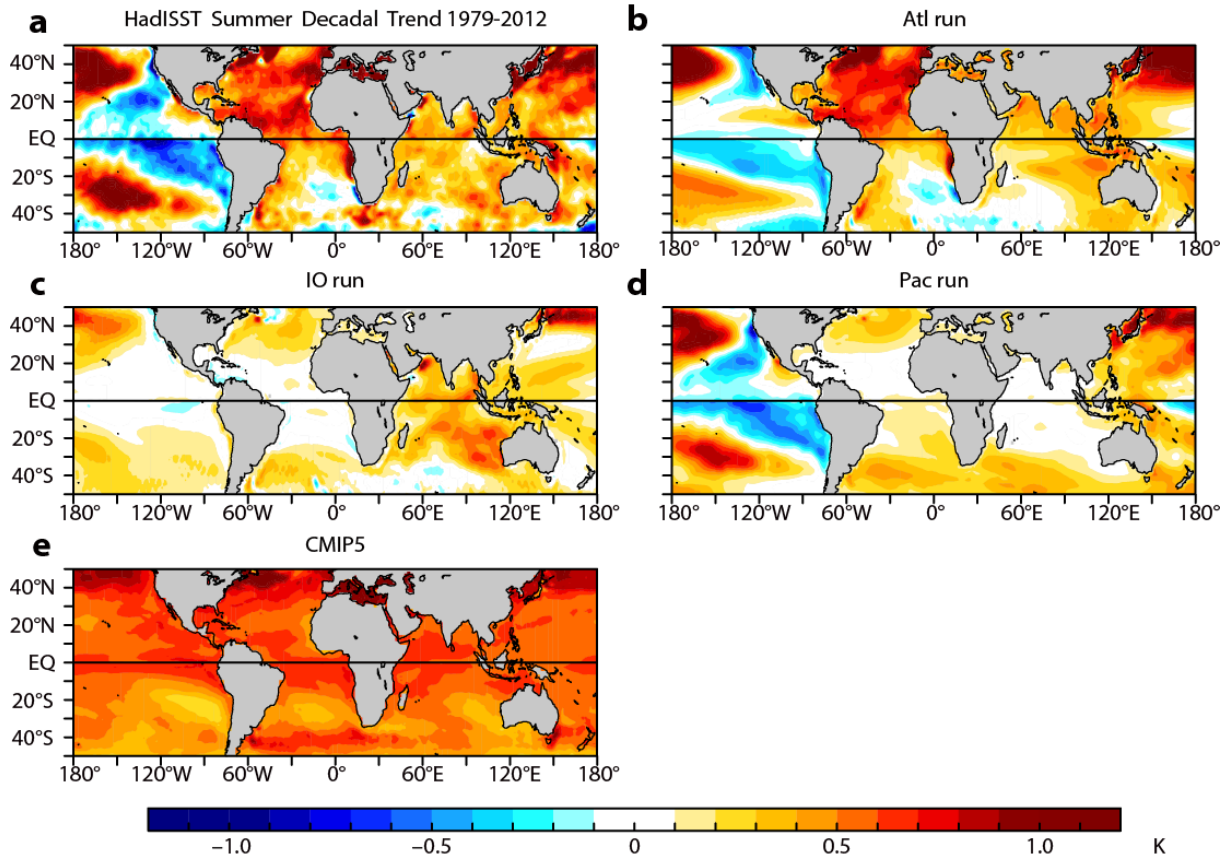

658

659

660 **Fig. 1** Decadal trends in summertime sea surface temperature (SST; K 34 yr^{-1}) for 1979–2012. Averages for May
661 to September and November to March are shown in the Northern and Southern Hemispheres, respectively.
662 Three-year running means are applied before calculating linear trends. (a) Observed trend in HadISST. (b)
663 12-member ensemble means of Atl, (c) IO, and (d) Pac runs, respectively. (e) CMIP5 24-model ensemble
664 mean. Models used are listed in Table S1 in the online supplement

665

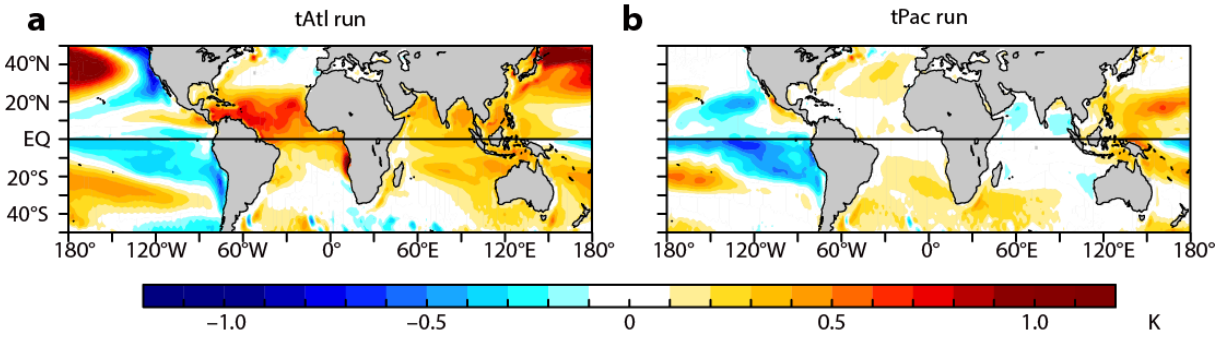

666

667

668 **Fig. 2** Similar to Fig. 1b–d but for (a) tAtl and (b) tPac runs, respectively

669

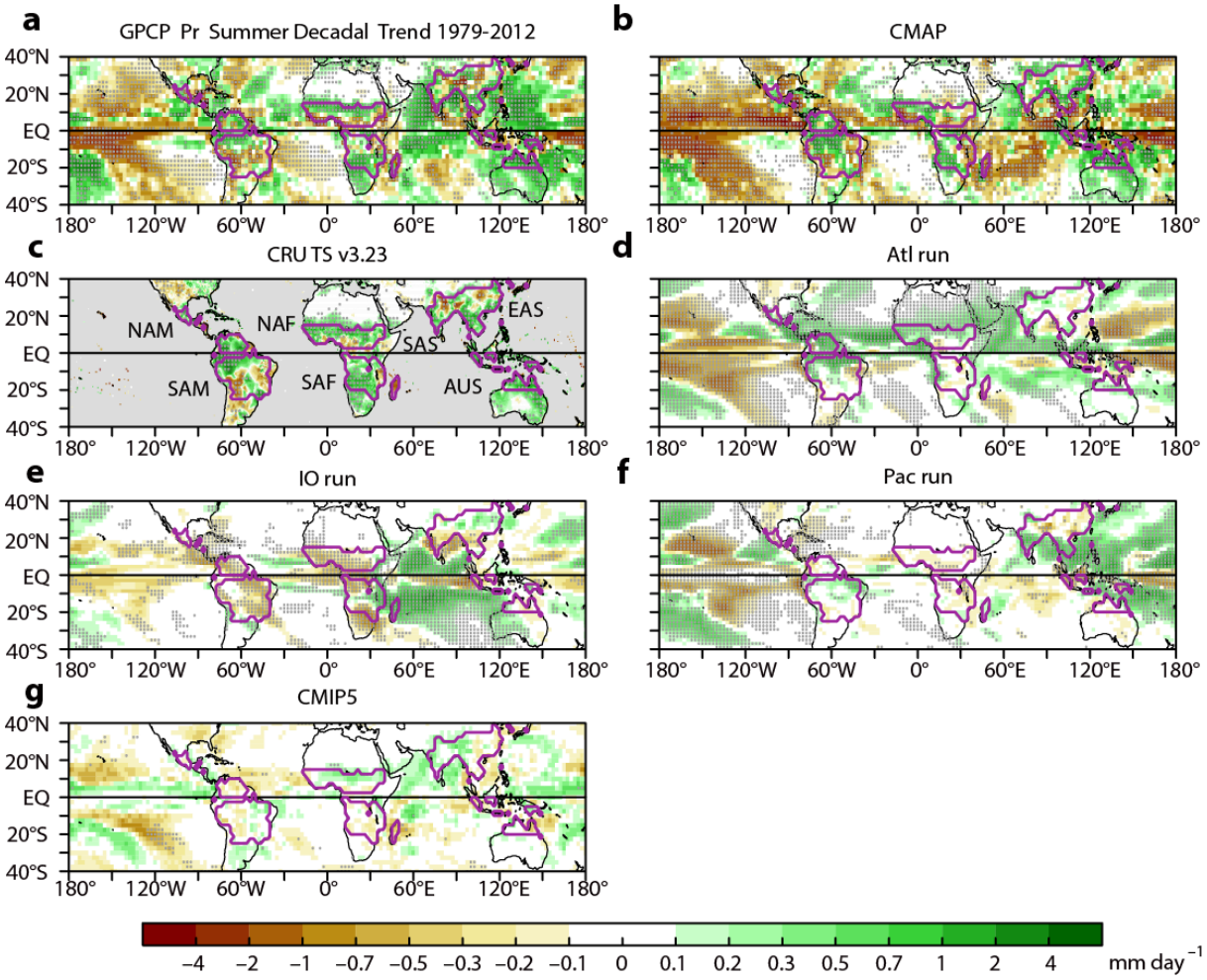

Fig. 3 Similar to Fig. 1 but for summertime precipitation (mm day^{-1} 34yr^{-1}). (a) Observed trends in GPCP, (b) CMAP, and (c) CRU TS v3.23. Stipples indicate areas with trends that are significant at the 95 % confidence level or higher. Areas surrounded by purple lines indicate land monsoon domains (North American Monsoon; NAM, South American Monsoon; SAM, North African Monsoon; NAM, South African Monsoon; SAM, South Asian Monsoon; SAM, East Asian Monsoon; EAM, Australian Monsoon; AUS). (d) Results of Atl, (e) IO, and (f) Pac runs, respectively. (g) 24-model mean of the CMIP5 multiple model ensemble

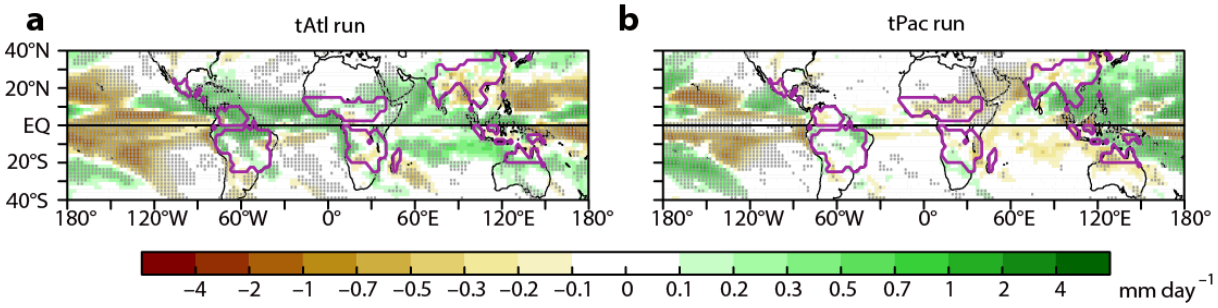

681

682

683 **Fig. 4** Similar to Fig. 2d–f but for (a) tAtl and (b) tPac runs, respectively

684

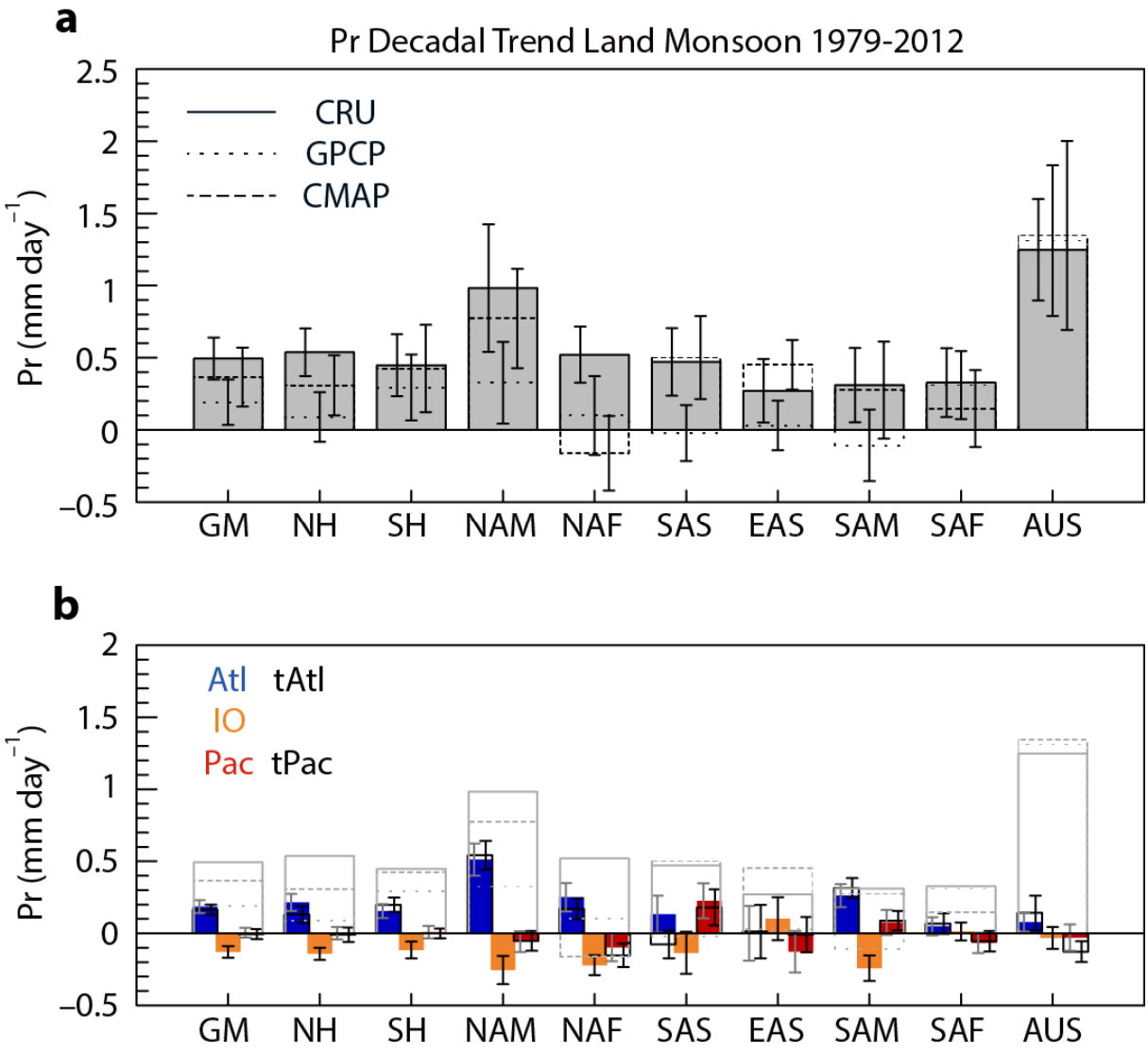

685

686

687 **Fig. 5** Decadal trends in summertime precipitation (mm day^{-1} 34yr^{-1}) averaged over the global land monsoon
688 domain (GM), Northern and Southern Hemisphere monsoon domains (NH and SH), and individual monsoon
689 domains (purple areas shown in Fig. 3). (a) Observed trends in CRU TS v3.23 (grey bar with solid line),
690 GPCP (dotted line) and CMAP (dashed line). Three error bars indicate 95% confidence intervals for (left to
691 right) CRU, GPCP and CMAP, respectively. (b) Modeled trends in Atl (blue bar), IO (orange bar) and Pac
692 (red bar) runs. Black rectangles represent results of tAtl and tPac runs. Error bars indicate 95% confidence
693 intervals. Grey and black error bars on the blue (red) bars indicate Atl and tAtl (Pac and tPac) runs,
694 respectively. Solid, dotted and dashed grey rectangles are identical to (a)

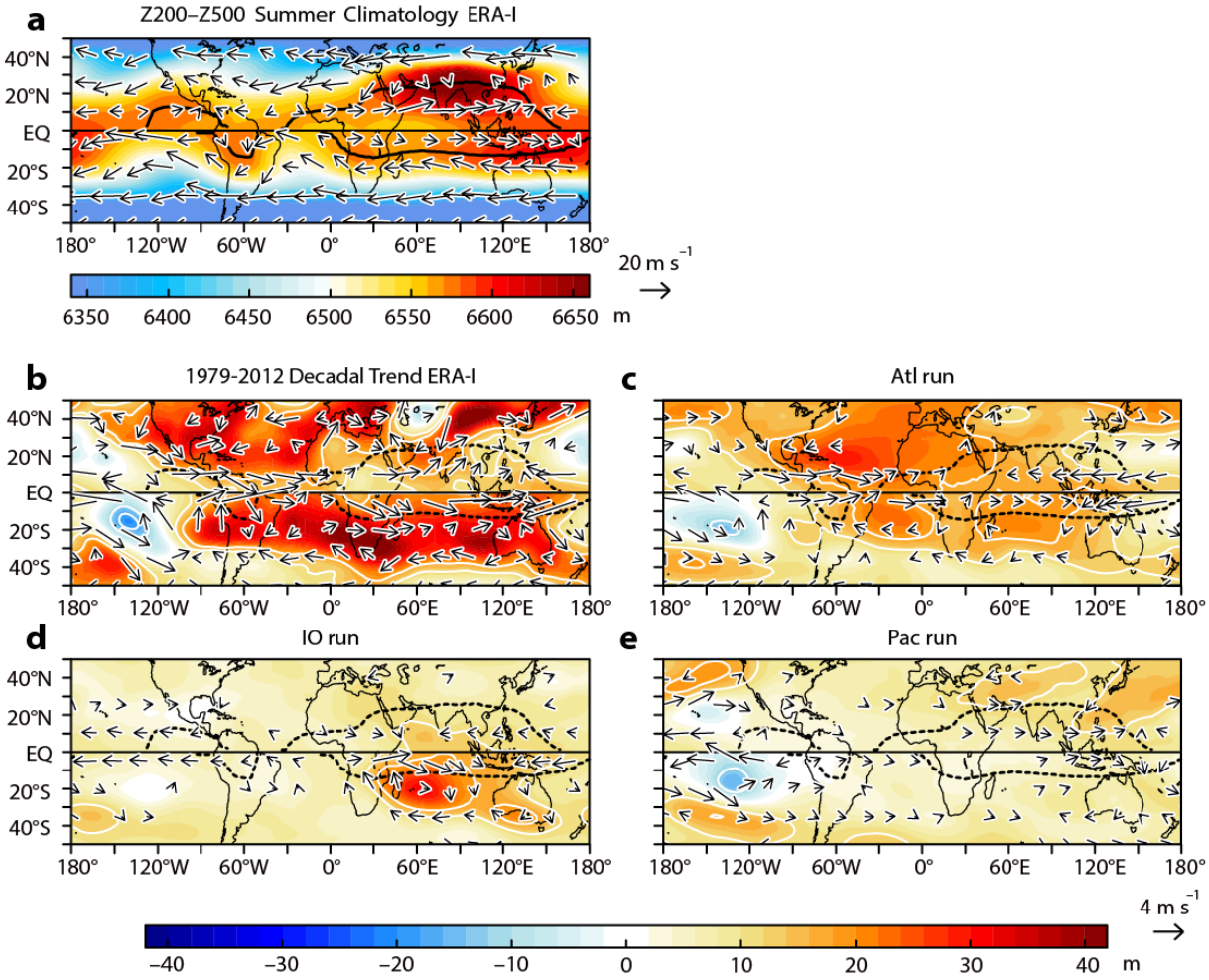

Fig. 6 Summertime mid-to-upper tropospheric thickness (Z200 minus Z500; shading; m) and vertical wind shear (850 hPa minus 200 hPa; vector; m s^{-1}). (a) Climatology for 1979–2012 in ERA-Interim. Thick black lines indicate latitudes with peak thickness in the individual hemispheres. (b) Decadal trend for 1979–2012 in ERA-Interim. Dashed lines represent the peak thickness in climatology, identical to the solid lines in (a). (c) Results of Atl, (d) IO, and (e) Pac runs, respectively

703 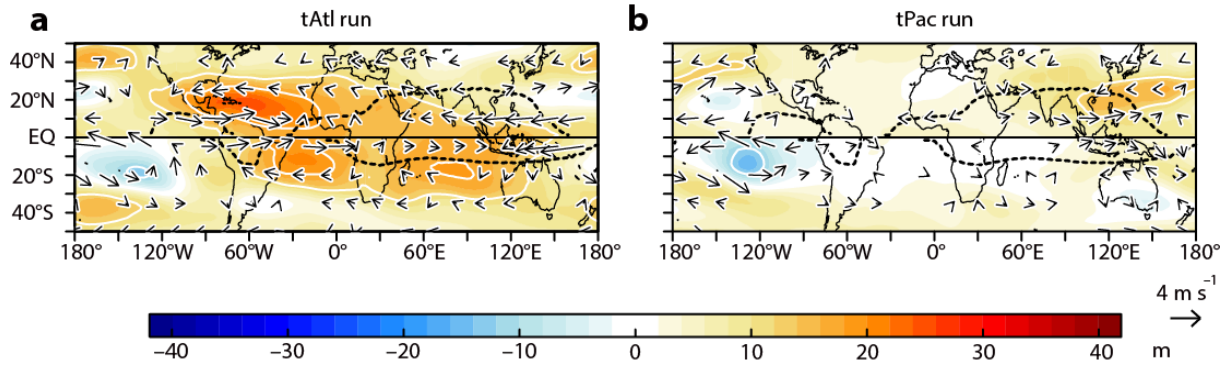

704

705 **Fig. 7** Similar to Fig. 6c–e but for (a) tAtl and (b) tPac runs, respectively

706

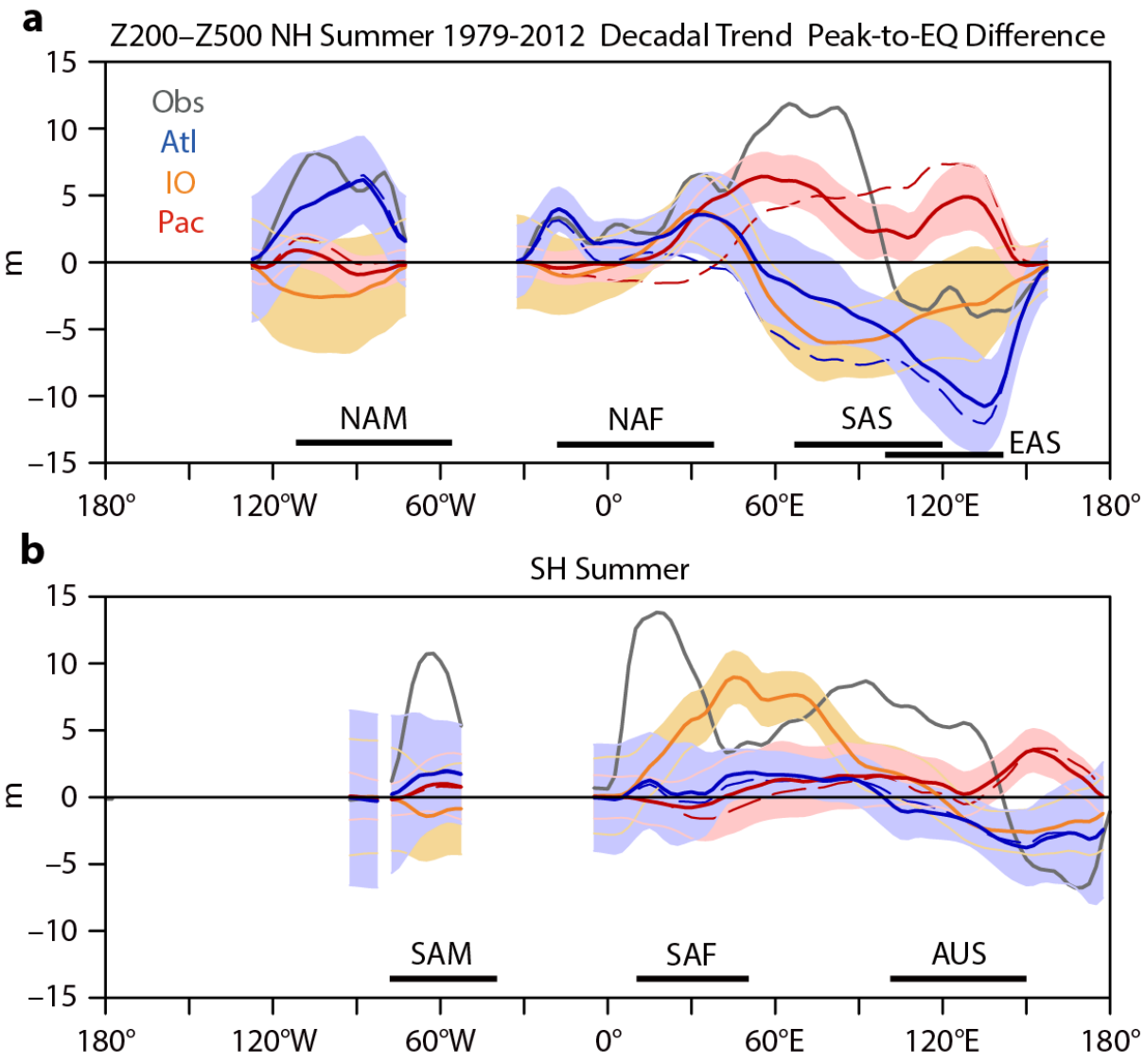

707

708

709 **Fig. 8** Difference in decadal trends of summertime mid-to-upper tropospheric thickness (Z200 minus Z500) for
710 1979–2012 (m 34yr^{-1}) between the peak latitude (black line in Fig. 6) and the equator. (a) ERA-Interim
711 (grey), Atl (blue), IO (orange), and Pac (red) runs over the Northern and (b) Southern Hemispheres,
712 respectively. Shadings represent 95% confidence intervals. Dashed blue and red lines indicate tAtl and tPac
713 runs, respectively. Black lines in the lower parts represent longitudinal areas of the land monsoon domains

714